Study of N_2O_2 by photoelectron spectroscopy of $N_2O_2^-$

Don W. Arnold[a] and Daniel M. Neumark[b]
Department of Chemistry, University of California, Berkeley, Berkeley, California 94720 and Chemical Sciences Division, Lawrence Berkeley Laboratory, Berkeley, California 94720

(Received 29 November 1994; accepted 31 January 1995)

Photoelectron spectra of the $N_2O_2^-$ anion, collected at $h\nu=4.657$ and 5.822 eV, are presented. The spectra originate from the C_{2v} isomer of the anion. Vibrationally resolved progressions corresponding to transitions to several electronic states of the previously unobserved N_2O_2 molecule are observed. All of the observed transitions lie above the dissociation asymptotes for N_2+O_2, NO+NO, and $O+N_2O$, and several lie above the $N+NO_2$ and N_2+O+O asymptotes. *Ab initio* calculations have been carried out for the anion ground state and several singlet and triplet states of neutral N_2O_2. By comparing the observed spectra with Franck–Condon simulations based on these calculations, the lowest bands observed in our spectra were assigned to transitions to the $^3A_2$ and $^3A_1$ states (C_{2v} symmetry) of N_2O_2. These spectra thus represent the first experimental characterization of metastable, high energy forms of N_2O_2. Both the $N_2O_2^-$ and the N_2O_2 species are considered in terms of their roles as reactive intermediates in the O^-+N_2O and $N+NO_2$ chemical reactions.© *1995 American Institute of Physics.*

I. INTRODUCTION

The widespread interest in nitrogen oxide chemistry results from the important roles which NO_x species play in combustion, atmospheric, and pollution chemistry.[1–4] The rather complex and interdependent nitrogen oxide cycles include both neutral and ion–molecule reactions. In many cases, the complexity of these reactions results from the availability of multiple product channels. Often several studies are necessary to determine which reactions actually occur under a specified set of experimental conditions.

As examples, consider the two reactions which are most closely related to the present study. Figure 1 is a schematic energetics diagram in which the primary channels are shown for the O^-+N_2O and $N+NO_2$ reactions. The reaction of the O^- anion with N_2O has been studied for many years. While there are several energetically accessible pathways for this reaction,

$$O^-+N_2O\rightarrow NO^-+NO \quad \Delta H=-2.8 \text{ kcal/mol}, \tag{1}$$

$$O^-+N_2O\rightarrow NO+NO+e^- \quad \Delta H=-2.3 \text{ kcal/mol}, \tag{2}$$

$$O^-+N_2O\rightarrow O_2^-+N_2 \quad \Delta H=-55.6 \text{ kcal/mol}, \tag{3}$$

$$O^-+N_2O\rightarrow O_2+N_2+e^- \quad \Delta H=-45.4 \text{ kcal/mol}, \tag{4}$$

only the first channel has been observed experimentally. This reaction was proposed[5,6] to proceed through a long-lived intermediate formed by the attack of an O^- anion onto either the central or terminal nitrogen atom of the N_2O, resulting in a C_{2v} NNO_2^- structure or an $ONNO^-$ structure, respectively. Recent studies of product distributions using isotopically labeled reactants support this proposed mechanism.[7,8] Anion photoelectron spectroscopy[9] and matrix isolation spectroscopy experiments[10–12] have established the existence of the two structures. Hence, the reaction coordinate for reaction (1) should resemble the diagram in the lower half of Fig. 1.

The $N+NO_2$ reaction has been studied using various kinetics techniques in order to determine the important channels and the product branching ratios. For this reaction, several channels are exothermic:

$$N+NO_2\rightarrow N_2O+O \quad \Delta H=-42 \text{ kcal/mol}, \tag{5}$$

$$N+NO_2\rightarrow NO+NO \quad \Delta H=-78 \text{ kcal/mol}, \tag{6}$$

$$N+NO_2\rightarrow N_2+O_2 \quad \Delta H=-121 \text{ kcal/mol}, \tag{7}$$

$$N+NO_2\rightarrow N_2+2O \quad \Delta H=-2 \text{ kcal/mol}. \tag{8}$$

Unlike the anion reaction considered above, kinetics measurements indicate that all four of the channels occur to some extent. The overall rate of reaction for ground state nitrogen atoms with nitrogen dioxide ($k_{\text{tot}}=1\times10^{-12}$–$2\times10^{-11}$ cm^3/molecule s) has been measured by various techniques.[13–16] The branching ratios for reactions (5)–(8) were determined to be 0.43 ± 0.04, 0.33 ± 0.07, 0.10 ± 0.12, and 0.13 ± 0.11, respectively, by Phillips and Schiff.[17] For the reaction of NO_2 with a combination of excited state $N(^2D)$ and $N(^2P)$ atoms, the branching ratio has been determined {1.00 (5); 0.65 (6) 0.27 [(7)+(8)]} but the overall reaction rate was determined to be much slower ($k_{\text{tot}}=3.3\times10^{-13}$ cm^3 molecule^{-1} s^{-1}) than for the ground state reaction.[18] Reactions (5)–(8) are also proposed to proceed via a mechanism whereby an attack onto the central nitrogen atom leads to the formation of an intermediate which decays to the various channels;[15] Fig. 1 qualitatively illustrates the energy along the reaction coordinate. No experiments have been performed to confirm this mechanism for the $N+NO_2$ reaction.

In recent years, we have used photoelectron spectroscopy of stable negative ions to probe the transition state region of direct, neutral bimolecular reactions.[19] Figure 1 suggests that the analogous experiment performed on $N_2O_2^-$ might be able to probe the reactive intermediate proposed for the $N+NO_2$ reaction. This paper describes the result of such a study. As this experiment is sensitive to the properties of

[a]Current address: Department of Chemistry, University of Southern California, Los Angeles, CA 90025.
[b]Camille and Henry Dreyfus Teacher–Scholar.

Downloaded 03 Mar 2005 to 128.32.220.150. Redistribution subject to AIP license or copyright, see http://ojps.aip.org/jcpo/jcpcr.jsp

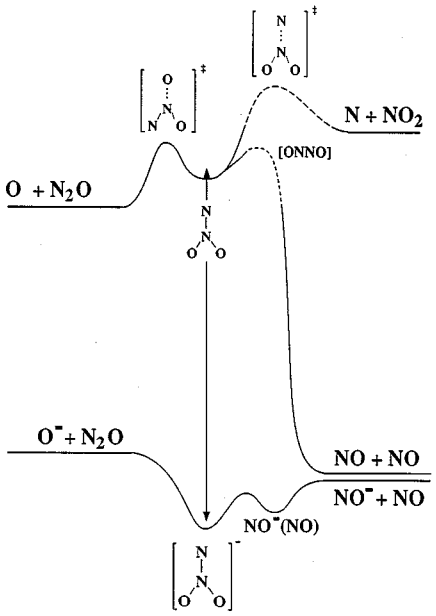

FIG. 1. Schematic energetics diagram for the O^-+N_2O and $N+NO_2$ reactions. The energies (not to scale) are shown as a function of generic reaction coordinates which are not the same for the two reactions.

the anion and neutral species, it is worthwhile to review in more detail what is known about each of these.

The $N_2O_2^-$ anion was first observed by Moruzzi and Dakin,[5] who found that the ion could be formed by the injection of electrons into a drift tube of N_2O at chamber pressures >0.3 Torr. Klots and Compton[20] and, more recently, Knapp *et al.*[21] generated $N_2O_2^-$ by low energy electron attachment to neutral N_2O clusters. Coe *et al.*[22] observed $N_2O_2^-$ by injecting electrons into the high pressure region of a free jet expansion of N_2O. Milligan and Jacox[10] recorded the first spectrum of $N_2O_2^-$ by infrared matrix isolation spectroscopy. From the observed frequencies and their isotopic dependence, the anion was determined to have a C_{2v} NNO_2^- structure. Further evidence for this structure was found in later matrix studies by Jacox[11] and by Hacaloglu *et al.*[12] These studies also identified a strongly bound $ONNO^-$ species.

The most detailed investigation to date of the $N_2O_2^-$ anion in the gas phase was an intriguing study by Posey and Johnson,[9] who obtained three very dissimilar and exclusive photoelectron spectra for the $N_2O_2^-$ anion by varying the starting materials used for ion formation. In their ion source, which is similar to the one used in the work reported here, a pulsed molecular beam crosses a 1 keV electron beam. Structure (I) was formed from a 5% O_2/N_2 gas mixture, structure (II) from a pure N_2O expansion, and structure (III) from a 10% NO/Ar mixture.[23] Structure (I) was identified by its photoelectron spectrum as O_2^- clustered to N_2. Structure II could not be photodetached at 3.495 eV, but was found to undergo photodissociation to O^-+N_2O. Structure (III) was photodissociated at 2.33 eV to give NO^-+NO. These results indicated that (II) and (III) were distinct, relatively strongly bound species. Based on the photodissociation products, the authors proposed that (II) was the C_{2v} form of the NNO_2^- anion and (III) was an isomer of the form $ONNO^-$, presumably the same isomer later identified by Jacox[11] and Hacaloglu *et al.*[12]

The results of Posey and Johnson imply that both (II) and (III) are intermediates in reaction (1), as illustrated in Fig. 1. Subsequent kinetics experiments by Barlow and Bierbaum[7] and Morris *et al.*[8] using totally labeled isotopic reactants (i.e., $^{18}O^-+{}^{14}N^{15}N^{16}O$) showed full scrambling in the reaction products, implying that the reaction indeed passes through both intermediates. For example, the observation of $^{18}N^{15}O^-+{}^{14}N^{16}O$ suggests that the reaction proceeds by a sequential process beginning with the O^- attack on the central N atom of the N_2O to form $[N_2O_2^-]$ in which the two oxygen atoms are equivalent. A rearrangement to form (III) is followed by dissociation into NO^- and NO in which the N atoms have lost knowledge of their origin. A recent *ab initio* study of several $N_2O_2^-$ isomers by Hiraoka *et al.*[24] predicts the C_{2v} geometry to be the ground state, with a *trans*-$ONNO^-$ isomer lying 4.4 kcal/mol higher in energy; this calculation is the basis for the relative well depths of the two minima in the lower half of Fig. 1.

In contrast to the moderate number of anion investigations, no experimental information on any form of N_2O_2 exists other than the weakly bound NO dimer.[25–28] However, there has been considerable theoretical interest in various metastable, high energy isomers of N_2O_2 due to their possible applications as high energy density materials. For example, an *ab initio* investigation by Michels and Montogomery[29] found that the $^1A_1$ electronic state of the $C_{2v}NNO_2$ structure is located at a potential energy minimum at the HF/6-31G* level of theory. However, there is only a very small barrier (2 kJ/mol) for rearrangement to a lower energy C_s structure of the form O–O–N–N. Several other high energy isomers have been proposed based on *ab initio* calculations.[30–32] These chemically bound forms of N_2O_2 have been proposed by Yang *et al.*[33] to play a role in the efficient vibrational energy transfer between two NO molecules when one is highly vibrationally excited.

In this paper, we make a further investigation of anion isomer (II), the C_{2v} geometry, and the corresponding neutral by a combination of anion photoelectron spectroscopy and *ab initio* calculations. By collecting photoelectron spectra of this anion at higher photon energies than used by Posey and Johnson,[9] we observe photodetachment transitions to several electronic states of the neutral species, NNO_2. The spectra contain much well-resolved vibrational structure, even though the observed spectral features lie well above the energetic asymptotes for dissociation of the N_2O_2 species. With the assistance of *ab initio* calculations for the anion and neutral, the bands in the photoelectron spectra are assigned to transitions to various electronic states of NNO_2. One of these states, the $^3A_2$ state, is a likely reactive intermediate in the $N+NO_2$ reaction. Overall, these results represent the first experimental observation and characterization of a high energy, metastable form of N_2O_2.

Downloaded¬03¬Mar¬2003¬to¬128.32.220.150. Redistribution¬subject¬to¬AIP¬license¬or¬copyright,¬see¬http://ojps.aip.org/jcpo/jcpcr.jsp

II. EXPERIMENT

A dual time-of-flight anion photoelectron spectrometer which has been previously described in detail[34] is employed for these experiments. The instrument is quite similar to that used by Posey and Johnson[9] in their study of $N_2O_2^-$. For the present experiments, $N_2O_2^-$ is generated at the intersection of a pulsed molecular beam and a 1 keV electron beam.[35] The molecular beam was operated by expanding neat N_2O at a backing pressure of ~1.5 bar through a 0.020 in. orifice at 20 Hz using a piezoelectric pulsed valve.[36] The $N_2O_2^-$ anions are believed to form through the mechanism outlined in Eqs. (9):

$$N_2O+e^-\rightarrow O^-+N_2, \tag{9a}$$

$$O^-+N_2O+M\rightarrow N_2O_2^-+M. \tag{9b}$$

After formation, the anions relax vibrationally and rotationally by collisions with the carrier gas atoms in the continuing molecular beam expansion.

The cooled ions are extracted into a Wiley–McLaren-type time-of-flight mass spectrometer[37] where they are separated by mass from other anions formed in the source region. The $N_2O_2^-$ anions are selectively photodetached by a properly timed 8 ns laser pulse. Photoelectron kinetic energies are determined by time-of-flight measurements through a 1 m field-free tube perpendicular to the anion velocity vector. The resolution of the apparatus is 8–10 MeV for electrons with 0.65 eV of electron kinetic energy (eKE) and degrades as $eKE^{3/2}$. For these experiments the fourth (266 nm; 4.657 eV; 15 mJ/pulse) and fifth harmonics (213 nm; 5.822 eV; 6 mJ/pulse) of a pulsed Nd:YAG laser are employed for photodetachment. The laser polarization angle can be rotated with respect to the direction of electron detection. In these experiments, the photoelectron spectra were relatively insensitive to polarization angle, and the data reported here were all taken at $\theta=90°$.

For experiments performed at 213 nm, scattered photons generate background signal through interactions with the surfaces in the detector region. A background spectrum, collected using the same laser power used during data collection, is fitted to a smooth function which is scaled and subtracted from the data to correct for the moderate level background.

III. RESULTS

A. Experiment

Figures 2 and 3 show the photoelectron spectra of $N_2O_2^-$ taken at photodetachment energies of 4.657 and 5.822 eV, respectively. The spectra represent the intensity of electron signal as a function of electron kinetic energy (eKE) where

$$eKE=h\nu-ADE(j)-E_v^0+E_v^-. \tag{10}$$

In Eq. (10), $h\nu$ is the photon energy and $ADE(j)$ is the adiabatic detachment energy to electronic state (j) of N_2O_2, i.e., the energy difference between the ground vibrational levels of the anion and the electronic state of N_2O_2 in question. E_v^0 and E_v^- represent in the vibrational energy (above the zero point) of N_2O_2 and $N_2O_2^-$, respectively. The instrument is calibrated by measuring the photoelectron spectra of the halide anions Cl^-, Br^-, and I^-.

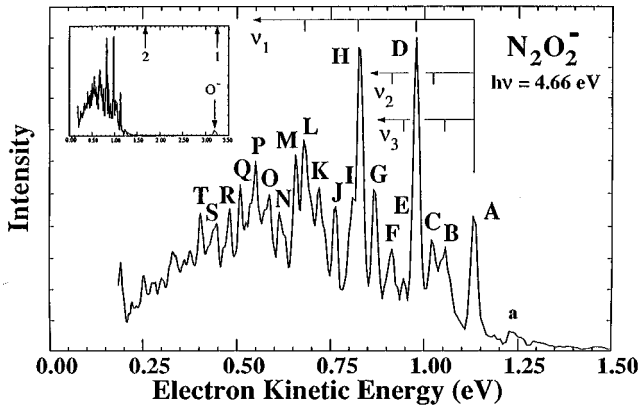

FIG. 2. Photoelectron spectrum of $N_2O_2^-$ collected at $h\nu=4.657$ eV. The inset points out the signal from O^- photodetachment that occurs after dissociation of $N_2O_2^-$. Also in the inset are arrows "1" and "2" indicating the NO+NO and O+N_2O dissociation asymptotes.

The 4.657 eV spectrum, Fig. 2, is a single band consisting of a well-resolved vibrational structure. The apparent origin is at eKE=1.126 eV. The peak positions are summarized in Table I. As indicated in Fig. 2, progressions in three different vibrational modes can be discerned in the data. The A,D,H,L progression is described by $\omega_e=1240$ cm^{-1} and $x_e\omega_e=7$ cm^{-1}. The other two modes have frequencies of 880 and 680 cm^{-1} and also appear to be quite anharmonic. Although the peaks are reasonably well resolved at the beginning of the band, the large number of resultant combination bands leads to congestion at lower eKE. The peak labeled "a" corresponds to photodetachment transitions originating from vibrationally excited anions. This assignment to a "hot band" is based upon the intensity dependence of this peak intensity upon the ion source conditions. The A–a separation provides an anion vibrational frequency of ~950 cm^{-1}; this

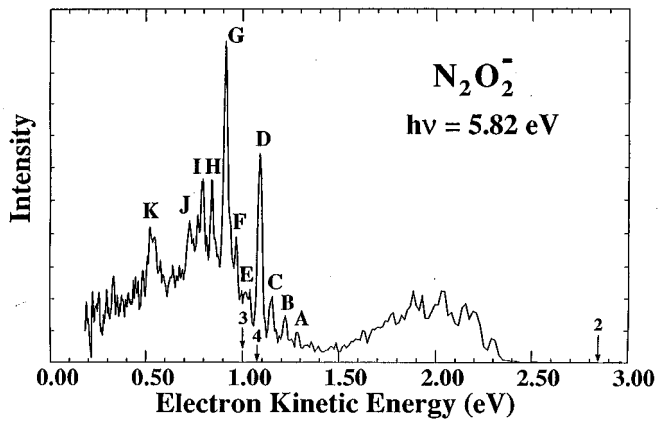

FIG. 3. Photoelectron spectrum of $N_2O_2^-$ collected at $h\nu=5.822$ eV. Arrows "2," "3," and "4" indicate the O+N_2O, N+NO_2, and N_2+O+O dissociation asymptotes.

Downloaded¬03¬Mar¬2003¬to¬128.32.220.150.¬Redistribution¬subject¬to¬AIP¬license¬or¬copyright,¬see¬http://ojps.aip.org/jcpo/jcpcr.jsp

TABLE I. Peak positions for 4.657 eV data.

Peak	Position (eKE)
A	1.126
B	1.055
C	1.016
D	0.969
E	0.942
F	0.905
G	0.861
H	0.820
I	0.795
J	0.755
K	0.711
L	0.671
M	0.649
N	0.613
O	0.586
P	0.549
Q	0.509
R	0.481
S	0.445
T	0.404

TABLE II. Peak positions for 5.822 eV data.

Peak	Position (eKE)
A	1.286
B	1.220
C	1.152
D	1.089
E	1.035
F	0.967
G	0.914
H	0.842
I	0.794
J	0.728
K	0.525

is close to the 1004 cm^{-1} vibration assigned to the C_{2v} isomer of $N_2O_2^-$ in a matrix.[11]

As labeled by an arrow marked "O^-" in the Fig. 2 inset, there is also a single peak in the $N_2O_2^-$ spectrum which is well separated from the other spectral features. This feature, located at 3.19 eV, corresponds to O^- photodetachment. The analogous feature was seen by Posey and Johnson[9] at a photodetachment energy $h\nu=2.33$ eV, and was assigned to a sequential two-photon process in which the $N_2O_2^-$ anion is photodissociated by the first photon to yield O^- and N_2O followed by photodetachment of the O^- by a second photon. This process apparently occurs at $h\nu=4.657$ eV as well. No peaks are observed at the eKEs where NO^- or O_2^- photodetachment signal is expected, indicating that dissociation of the $N_2O_2^-$ to yield NO^- or O_2^- does not occur at detectable levels at $h\nu=4.657$ eV. In agreement with the work of Posey and Johnson, we do not observe any signal corresponding to the $NO^-(NO)$ or the $O_2^-(N_2)$ species when N_2O is used as the starting material for $N_2O_2^-$ formation. Given this plus the agreement of the anion hot band with the frequency found by Jacox, we assign the spectrum in Fig. 2 to photodetachment from the C_{2v} isomer of the $N_2O_2^-$ isomer.

According to Fig. 1 and Eq. (11), the measured eKE of a photoelectron can be related to the asymptotic energy of the N_2O_2 dissociation products,

$$\mathrm{eKE}=h\nu-D_0^-(\mathrm{EA}_{\mathrm{prod}})-E_{\mathrm{int}}^0+E_{\mathrm{int}}^-. \tag{11}$$

Here, D_0^- is the dissociation energy of $N_2O_2^-$ into neutral and anion fragments, the latter of which has an electron affinity of $\mathrm{EA}_{\mathrm{prod}}$. The other terms are the same as for Eq. (10). Thus, the eKE distribution provides information about the energetic stability of N_2O_2 with respect to various dissociation pathways.

The energetic asymptotes for dissociation of the N_2O_2 molecule calculated using Eq. (11) are shown along the top axis of the Fig. 2 inset. Arrow "1" at eKE=3.25 eV indicates the NO+NO limit and arrow "2" at eKE=1.69 eV represents the $O+N_2O$ asymptote. These values are determined using Eq. (11), known reaction exothermicities, and an upper limit of 1.43 eV for $N_2O_2^-$ dissociation to O^-+N_2O; this limit for $D_0(O^-\cdots N_2O)$ has been recently determined in a separate experiment performed in our laboratory which will be described briefly in Sec. IV B. Thus, all of the observed vibrational features lie above both of these asymptotes, suggesting that significant barriers exist along both dissociation coordinates for the N_2O_2 molecule.

In the 5.822 eV photoelectron spectrum of $N_2O_2^-$, Fig. 3, the features of the band observed in Fig. 2 are significantly broadened due to the poorer resolution at higher eKE. The arrows marked 2, "3," and "4" indicate the $O+N_2O$, $N+NO_2$, and N_2+O+O dissociation asymptotes, respectively. Beginning at eKE=1.286 eV, a second set of spectral features appears in the spectrum. In general, the peaks are unevenly spaced and appear to result from overlapping transitions to multiple electronic states of N_2O_2. The peak positions are summarized in Table II. In addition to the 540 cm^{-1} progression (A–C) beginning at 1.286 eV, there are two dominant narrow features at 1.089 and 0.914 eV which do not appear to belong to a single vibrational progression. There are several smaller features that seem to belong to vibrational progressions beginning at A, D, and perhaps G. There is also a significantly broader feature, "*K*," which occurs at ~0.525 eV with a width of ~60 MeV (i.e., much broader than the experimental resolution of ~10 MeV in this energy region).

Due to the relatively low cross section for photodetachment and the competition with the photodissociation process described above, it was necessary to use unusually high ion densities in order to obtain a reasonable signal-to-noise ratio. At these higher ion levels the energy of the photodetached electron is affected by Coulombic interactions with the remaining undetached ions in the laser interaction region. This interaction shifts the spectrum to higher eKE and broadens the observed spectral features. The magnitude of the "space-charge shift" is determined by the measurement the shift experienced by calibration ions at the same ion densities used for the $N_2O_2^-$ data collection. Through this procedure, we find the data to be shifted by ~8 MeV and peaks to be broadened by ~2–3 MeV. The energy axis of the spectra in Figs. 2 and 3 has been corrected accordingly.

Downloaded¬03¬Mar¬2003¬to¬128.32.220.150. Redistribution¬subject¬to¬AIP¬license¬or¬copyright,¬see¬http://ojps.aip.org/jcpo/jcpcr.jsp

TABLE III. *Ab initio* results for $N_2O_2^-$ anion.[a]

Theory	Energy	R_{N-N}	R_{N-O}	R_{O-O}	∠ONO	ω_1	ω_2	ω_3	ω_4	ω_5	ω_6
UHF/6-31+G*	−258.494 495	1.253	1.254	2.189	121.6°	1582	1086	692	836	1434	654
MP2/6-31+G*	−259.178 980	1.270	1.253	2.164	119.4°	1411	1241	679	998	1538	609
Expt.											
Ar matrix[b]	⋯	⋯	⋯	⋯	⋯	1356	1004	⋯	⋯	1199	⋯
Ne matrix[c]	⋯	⋯	⋯	⋯	⋯	1359	1008	⋯	⋯	1205.5	⋯

[a]Bond lengths in Å, energy in a.u. (hartrees) and vibrational frequencies in cm^{-1}. See Fig. 4 for parameter definitions.
[b]References 11 and 12.
[c]Reference 11.

B. *Ab initio* calculations

For assistance in the assignment of the photoelectron spectra, *ab initio* calculations for $N_2O_2^-$ and N_2O_2 have been performed using the GAUSSIAN 92 package.[38] The standard 6-31+G* basis is employed in spin-unrestricted HF and MP2 calculations of the optimized geometries and vibrational frequencies. The anion results, discussed first in Sec. III B 1, will be followed by a discussion of calculations for the lowest N_2O_2 singlet state and four N_2O_2 triplet states.

1. $N_2O_2^-$ calculations

In C_{2v} symmetry, the $N_2O_2^-$ ground state is predicted to be the $^2B_2$ state with the orbital occupation $(\cdots 4b_2^2 2b_1^2 8a_1^2 1a_2^2 5b_2^1)$. Investigations of other possible anion electronic states (i.e., $^2A_2$, $^2B_1$, and $^2A_1$ in C_{2v} symmetry and the $^2A''$ state in C_s symmetry) at the HF/6-31+G* level of theory show that they lie higher in energy. Support for this assignment is found by comparison with the isoelectronic NO_3 and FCO_2 molecules. Weaver *et al.*[39] assign the ground state of the D_{3h} symmetric NO_3 molecule as the $\tilde{X}\ ^2A_2'$ state which, as Walsh shows,[40] correlates to the $^2B_2$ state in the C_{2v} point group. The ground state of the isoelectronic FCO_2 radical has also been assigned as the $\tilde{X}\ ^2B_2$ electronic state.[41,42]

As shown in Table III, the geometry optimizations at both the HF/6-31+G* and the MP2/6-31+G* levels of theory predict a C_{2v} symmetric species with three nearly equal bond angles and bond lengths; these results differ slightly from the spin-restricted HF calculation by Hiraoka[24] which found the N–O bonds to be 0.05 Å longer than the N–N bond. The geometrical parameters are illustrated in Fig. 4(a). Note that the calculated R_{N-N} is characteristic of a N–N double bond; $R_{N-N}=1.252$ Å in N_2H_2, for example.[43] The $N_2O_2^-$ vibrational frequencies have also been calculated at both levels of theory. The results agree reasonably well with the experimental $N_2O_2^-$ vibrational frequencies measured in the matrix isolation experiments.[10–12] Through a force constant analysis of these vibrational frequencies, Hacaloglu *et al.*[12] estimate the ∠ONO angle of $N_2O_2^-$ to be between 105° and 120°. The angle is calculated to be 119.2° and 120.3° at the HF and MP2 levels of theory, respectively.

2. N_2O_2 calculations

In the case of the neutral N_2O_2 molecule, several electronic states which can be produced by one-electron photodetachment of the $N_2O_2^-$ anion were investigated. We first looked at the state resulting from removal of the $5b_2$ electron from $N_2O_2^-$ since this forms the closed shell $^1A_1$ state of N_2O_2 in C_{2v} symmetry. The geometry optimization of the N_2O_2 species with this orbital occupation provided rather interesting results which are summarized in Table IV. When the N_2O_2 molecule was constrained to have C_{2v} symmetry, two stationary points were located on the potential energy surface. Force constant analyses revealed that one of these geometries was located at a potential energy minimum while the other was a first-order transition state with an imaginary frequency for the NO_2 antisymmetric stretch.

At the potential energy minimum, the $^1A_1$ state [structure (B) in Table IV] is similar to that determined by Michels[29] at the HF/6-31+G* level of theory. The geometry obtained at the MP2/6-31+G* level of theory is very close to the C_{2v} structure recently calculated by Nguyen *et al.*[32] at the MP2 level with a somewhat different basis set.[44] Our MP2 calculation shows that a significant interaction exists between the

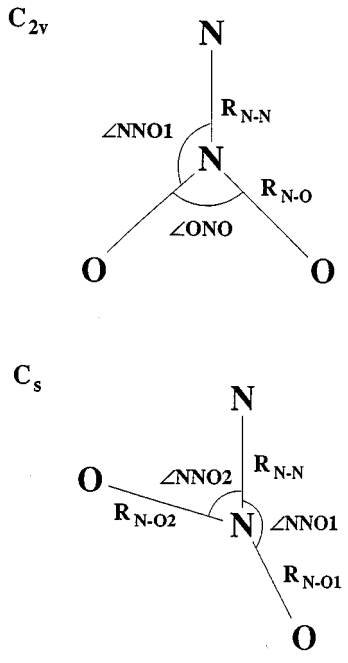

FIG. 4. Definition of parameters used in calculation of *ab initio* geometries for the C_{2v} (top) and C_s (bottom) species.

Downloaded¬03¬Mar¬2003¬to¬128.32.220.150.¬Redistribution¬subject¬to¬AIP¬license¬or¬copyright,¬see¬http://ojps.aip.org/jcpo/jcpcr.jsp

TABLE IV. *Ab initio* results for N_2O_2 singlet calculations.[a]

State		HF/6-31+G*	MP2/6-31+G*	Mode	HF/6-31+G*	MP2/6-31+G*
			C_{2v} symmetry			
$^1A_1$	R_{N-N} (Å)	1.302	1.253	ω_1	1535	1415
(A)	R_{N-O} (Å)	1.190	1.243	ω_2	1178	1121
	R_{O-O} (Å)	2.169	2.276	ω_3	692	575
	∠ONO	131.4°	132.6°	ω_4	876	728
	Energy	−258.332 951	−259.014 352	ω_5	1761	1696
				ω_6	176**i**	824**i**
$^1A_1$	R_{N-N} (Å)	1.127	1.138	ω_1	2197	2358
(B)	R_{N-O} (Å)	1.350	1.494	ω_2	1179	1155
	R_{O-O} (Å)	1.478	1.592	ω_3	895	628
	∠ONO	66.4°	64.4°	ω_4	510	520
	Energy	−258.293 541	−259.030 722	ω_5	668	1089
				ω_6	459	165
			C_s symmetry			
$^1A'$	R_{N-N} (Å)	1.202	1.242	ω_1	2029	2190
	R_{N-O1} (Å)	1.168	1.231	ω_2	1390	1237
	R_{N-O2} (Å)	1.313	1.460	ω_3	1098	1005
	∠NNO1	146.6°	152.7°	ω_4	657	631
	∠NNO2	80.0°	73.2°	ω_5	468	304
	Energy	−258.341 391	−259.070 351	ω_6	733	534

[a]Bond lengths given in Å, energy in au (hartree), and vibrational frequencies in cm^{-1}. See Fig. 4 for parameter definitions.

two oxygen atoms; the ONO angle is only 64° and the O–O separation is only 1.59 Å (vs 1.475 Å in H_2O_2,[45] for example). In $N_2O_2^-$, the O–O antibonding character of the $5b_2$ orbital hinders such bonding and results in the considerably larger ∠ONO angle for the anion (~120° from Table III). The extreme difference in the geometries of this neutral state and the anion ground state is important when trying to assign bands in the photoelectron spectrum.

At the other stationary point, the saddle point species is calculated to lie 0.44 eV above the C_{2v} minimum at the MP2/6-31+G* level of theory. Upon removal of the C_{2v} symmetry constraint, the saddle point species relaxes significantly to a $C_s(^1A')$ structure with one acute NNO angle and one obtuse NNO angle. One of the NO bond lengths is significantly longer (1.49 Å) than the other (1.14 Å). This C_s minimum energy structure lies 1.52 eV below the saddle point geometry and 1.08 eV below the C_{2v} minimum at the MP2/6-31+G* level of theory. Force constant analyses at each stationary point yield the frequencies shown in Table IV. This species is distinct from the *a*-N_2O_2 geometry calculated by Michels and Montgomery,[29,32] thus showing that yet another minimum exists on the N_2O_2 potential energy surface.

Removal of an electron from the $1a_2$, $8a_1$, $4b_2$, or $2b_1$ orbitals of $N_2O_2^-$ results in open shell singlet and triplet states with B_1, B_2, A_1, or A_2 electronic symmetries, respectively. For the present analysis, only the triplet states will be considered. Preliminary investigations of the open-shell singlet states by unrestricted Hartree–Fock methodology were found to suffer from significant spin contamination. While further calculations are not pursued here, additional discussion of the singlet states is given in Sec. IV. The triplet states that can result from $N_2O_2^-$ photodetachment were investigated at the HF and MP2 levels just as for the closed-shell singlet states discussed above. A summary of the geometry optimizations and vibrational frequency calculations for the triplet states is given in Table V. At the HF/6-31+G* level of theory, all listed geometries correspond to potential energy minima. However, the MP2/6-31+G* force constant analysis indicates that the $^3B_1$ state is located at a saddle point. Since this saddle point lies ~3 eV above the $^3A_2$ state and the other three states are located at potential energy minima (at both levels of theory), no investigations were made of C_s geometries for the triplet states.

A comparison of Tables III and V shows that ∠ONO is the geometrical parameter that varies the most upon photodetachment to the triplet states. R_{N-N} does not change very much upon photodetachment to the $^3A_1$, $^3B_1$, and $^3B_2$ states, so the N–N bond in these states is basically a double bond just as in the anion. However, R_{N-N} for the $^3A_2$ state is 0.17 Å longer than in the anion. The calculated values of 1.405 Å (HF) and 1.441 Å (MP2) are characteristic of a N–N single bond; R_{N-N}=1.449 Å in N_2H_4.[46]

At the HF level, the calculations result in the $^3A_1 < ^3A_2 < ^3B_1 < ^3B_2$ energetic ordering of the electronic states. Inclusion of electron correlation at the MP2 level changes the ordering to $^3A_2 < ^3A_1 < ^3B_2 < ^3B_1$. Due to this reordering as a result of electron correlation, further investigation of the energies of the triplet states relative to each other, to the singlet states, and to the anion were made by calculating the MP4/6-311+G* energy for each state at their respective MP2/6-31+G* optimized geometries. This results in a $^3A_2 < ^3A_1 < ^3B_1 < ^3B_2$ ordering of the states. From these results the adiabatic electron detachment energies (ADEs) have been calculated for each state.[47] A listing of these energies is given in Table VI. A zero-point corrected energy is also given for each ADE where the zero-point energy is determined from the calculated vibrational frequencies. At this

Downloaded¬03¬Mar¬2003¬to¬128.32.220.150. Redistribution¬subject¬to¬AIP¬license¬or¬copyright,¬see¬http://ojps.aip.org/jcpo/jcpcr.jsp

TABLE V. *Ab initio* results for N_2O_2 triplet calculations.[a]

$^3A_2$	Energy	R_{N-N}	R_{O-O}	R_{N-O}	∠ONO	ω_1	ω_2	ω_3	ω_4	ω_5	ω_6
UHF/6-31+G*	−258.413 572	1.405	2.143	1.185	129.4	1576	1050	716	777	1868	565
MP2/6-31+G*	−259.059 695	1.441	2.228	1.230	129.8	1431	902	625	638	1815	483
$^3A_1$											
UHF/6-31+G*	−258.425 991	1.225	2.015	1.270	105.0	1543	1038	608	608	1288	576
MP2/6-31+G*	−258.997 166	1.182	1.994	1.294	100.8	1972	1142	649	819	1776	585
$^3B_2$											
UHF/6-31+G*	−258.341 850 7	1.144	2.217	1.388	106.0	2037	869	495	618	977	561
MP2/6-31+G*	−258.953 920 3	1.188	2.344	1.311	126.8	1646	959	611	541	1164	312
$^1B_1$											
UHF/6-31+G*	−258.375 947	1.282	2.166	1.280	115.6	1634	1032	657	437	923	545
MP2/6-31+G*	−258.951 237	1.248	2.167	1.301	112.8	1467	1022	618	627	571	1180**i**

[a]Bond lengths given in Å, energy in a.u. (hartree) and vibrational frequencies in cm^{-1}. See Fig. 4 for parameter definitions. For the $^3A_2$ electronic state, ν_1 is the NO symmetric stretch (s.s.), ν_2 is the NN s.s. and ν_3 is the NO_2 bend. For the other three states, ν_1 is the NN s.s., ν_2 is the NO s.s. and ν_3 is the NO_2 bend.

level of theory, we see that the $^1A'$ and $^3A_2$ states are separated (including the zero-point energy correction) by only 81 MeV, so the actual energy ordering is unclear.

Table VI also includes vertical detachment energies (VDEs) determined by calculating the MP4/6-311+G* energy of each electronic state at the MP2/6-31+G* optimized geometry of the $N_2O_2^-$ anion. The VDEs for the $^1A'$ and $^1A_1$ states are identical because the latter is actually a local minimum (structure B in Table IV) on the same electronic surface as the $^1A'$ state. At this level of calculation, the C_{2v} saddle point on the singlet surface (structure A) is 0.27 eV lower in energy than structure B, and the ADE to the $^1A_1$ minimum is higher than the VDE because the anion geometry is much closer to structure A than structure B. Again, it appears that additional electron correlation does affect the relative energies of the species, suggesting that calculations beyond those presented here are required to determine the actual ordering of the stationary points on the potential energy surfaces.

IV. ANALYSIS AND DISCUSSION

As described in Sec. III, the spectra represent photodetachment transitions from the C_{2v} $N_2O_2^-$ anion to more than one electronic state of the N_2O_2 molecule. The next step in the data analysis is the identification of the final states involved in the photodetachment transitions. As discussed in Sec. III B 2, photodetachment of an electron from any of the four highest-lying orbitals of the $N_2O_2^-$ anion can produce N_2O_2 electronic states of all four symmetries associated with the C_{2v} point group. The data provide two types of information which can be used to make the assignments: (1) the energies of the electronic states and (2) the vibrational structure within each electronic band. The state energetics can be compared directly to the *ab initio* calculations. Within each electronic band, the peak spacings are determined by the vibrational frequencies in the neutral, and the intensity distribution by the Franck–Condon factors for photodetachment. The latter depend upon a combination of the geometry change upon photodetachment and the vibrational force constants of both the anion and neutral.

In the following sections, the photoelectron spectra will be considered in more detail. In Sec. IV A, Franck–Condon simulations based on the *ab initio* calculations described above will be compared with experiment, leading to proposed assignments of the spectral features to states of the N_2O_2 molecule. Our results will then be considered in Sec. IV B with reference to the role of $N_2O_2^-$ and N_2O_2 as metastable reactive intermediates in the $O^- + N_2O \rightarrow NO^- + NO$ and $N + NO_2 \rightarrow O + N_2O$ reactions, respectively, as well as the possible role of N_2O_2 in the vibrational relaxation of highly excited NO.

A. Franck–Condon analysis

From the calculated geometries and force constants for $N_2O_2^-$ and N_2O_2, one can simulate the *ab initio* vibrational profiles which are expected for photodetachment to the N_2O_2 electronic states. The photodetachment transition intensity, I, for the process

$$N_2O_2^-(v_1'', v_2'', v_3'') \xrightarrow{h\nu} N_2O_2(v_1', v_2', v_3') + e^-$$

TABLE VI. Calculated electron detachment energies.[a]

State	ADE[b]	ADE+ZPE[c]	VDE[d]
$^1A'$	2.907	2.871	4.024[e]
$^3A_2$	2.916	2.952	3.409
$^1A_1$	4.033	4.068	4.024[e]
$^3A_1$	4.278	4.250	4.783
$^3B_1$	5.172	5.109[f]	5.414
$^3B_2$	5.252	5.329	5.394

[a]MP4/6-311+G* energy calculated at the MP2/6-31+G* optimized geometry. All energies in eV.
[b]Adiabatic detachment energy.
[c]ADE plus zero-point energy (ZPE) correction using MP2/6-31+G* vibrational frequencies.
[d]Vertical detachment energy.
[e]These values are the same because the $^1A_1$ electronic state lies along the C_{2v} seam of $^1A'$ potential energy surface.
[f]ZPE correction made using the HF/6-31+G* frequencies because an imaginary frequency results at the MP2/6-31+G* level.

Downloaded¬03¬Mar¬2003¬to¬128.32.220.150. Redistribution¬subject¬to¬AIP¬license¬or¬copyright,¬see¬http://ojps.aip.org/jcpo/jcpcr.jsp

is calculated according to Eq. (12)

$$I \propto v_e |\tau_e|^2 \prod_{i=1}^{6} |\langle \psi_{v_i'}(Q_i) | \psi_{v_i''}(Q_i) \rangle|^2, \tag{12}$$

where v_e is the asymptotic velocity of the photodetached electron and τ_e is the electronic transition dipole which is considered to be a constant for each electronic state. In the separable parallel normal mode approximation, the Franck–Condon factors (FCFs) for each vibrational mode, $|\langle \psi_{v_i'}(Q_i) | \psi_{v_i''}(Q_i) \rangle|^2$, are calculated as the spatial overlap of the vibrational wave functions of the anion, $\psi_{v_i''}$, and the neutral, $\psi_{v_i'}$, for that mode. For each N_2O_2 electronic state, the normal coordinate displacements between the anion and neutral are obtained by standard matrix methods using the *ab initio* Cartesian force constant matrix and the optimized geometries for the anion and neutral. The resultant stick spectrum is convoluted with the experimental resolution function for comparison to the experimental data.

In general, a photodetachment transition between an anion and a neutral possessing the same symmetry (i.e., C_{2v}) will only excite totally symmetric vibrational modes of the neutral. In the case of the C_{2v} geometry, there are three symmetric modes, best labeled as the NN stretch, the NO stretch, and the NO_2 bend. For the other three nonsymmetric normal modes, only transitions to even vibrational levels of the neutral from the anion ground state have nonzero Franck–Condon overlap. Significant excitation of these modes occurs only if there is a very large difference in the anion and neutral vibrational frequencies for that mode. If the neutral state has C_s symmetry, such as the singlet structure in Table IV, there are five totally symmetric modes to consider; only the out-of-plane ν_6 mode is not totally symmetric.

According to Eq. (12), the length of a vibrational progression observed in anion photoemission spectroscopy depends, in general, upon the difference in geometry between the anion and the neutral. A significant geometrical rearrangement upon photodetachment results in a long vibrational progression, whereas if the anion and neutral have very similar geometries, the spectrum is dominated by the 0–0 transition. In the case of photodetachment transitions to the $^1A_1$ state, the geometry change is so dramatic (i.e., the $\angle$ONO angle changes by 56° at the MP2 level), that the Franck–Condon intensity is extremely spread out over many vibrational levels for this state. A similar situation occurs for the $^1A'$ state in which one of the NNO angles changes by 47°. This suggests that the relatively compact vibrational progressions we observe in the photoelectron spectra are not due to transitions to these singlet states. The other N_2O_2 geometries considered by Nguyen *et al.*[32] are also unlikely candidates, as their geometries differ even more from the C_{2v} anion structure.

The geometries of the triplet states listed in Table V, however, are much closer to that of the anion. Figure 5 shows the Franck–Condon simulations for the $^3A_1$, $^3A_2$, $^3B_1$, and $^3B_2$ electronic states using the results of the HF *ab initio* calculated geometries and neutral force constants. In the simulations, the 0–0 transition is placed at 1.126 eV for purposes of comparison with the 4.657 eV photoelectron spectrum. Each state has its own characteristic profile. While the $^3B_1$ state is dominated by the 0–0 transition, the other three states have reasonably long progressions in at least one vibrational mode. The $^3A_1$ state primarily has a long progression in the NO_2 bending mode with a slight excitation of the NN stretch (ν_1), while the $^3A_2$ state is dominated by the NO and NN stretches (ν_1 and ν_2, respectively), with much less excitation in the NO_2 bend (ν_3). The $^3B_2$ spectrum is also dominated by stretching progressions, with considerably more excitation in these modes than in the $^3A_2$ spectrum leading to significant congestion at low eKE.

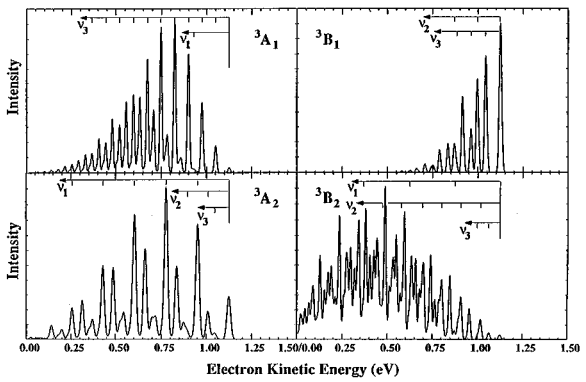

FIG. 5. *Ab initio* simulations at HF/6-31+G* level for the $N_2O_2^-$ photoelectron transitions to the triplet electronic states of N_2O_2 molecule.

Figure 6 shows the simulations of the photoelectron spectrum using the MP2 calculated geometries and force constants. The different equilibrium geometries and force constants which result from the MP2 calculations can result in very different simulated spectra relative to the HF simulations. The greatest change occurs in the $^3B_2$ simulation where a larger than average electron correlation effect is observed in the geometry calculation. In this case, activity in the ν_2 mode (NO stretch) is greatly decreased relative to the HF simulation, and the most prominent progression is in the ν_3 bend mode. The appearance of the $^3A_2$ simulation is also quite different, although progressions in the ν_1 and ν_2

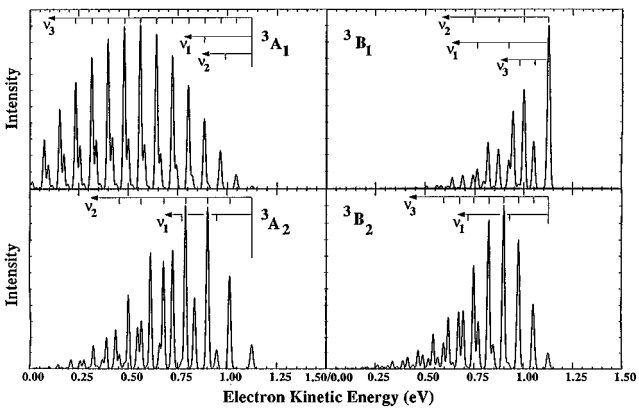

FIG. 6. *Ab initio* simulations at MP2/6-31+G* level for the $N_2O_2^-$ photoelectron transitions to the triplet electronic states of N_2O_2 molecule.

Downloaded¬03¬Mar¬2003¬to¬128.32.220.150. Redistribution¬subject¬to¬AIP¬license¬or¬copyright,¬see¬http://ojps.aip.org/jcpo/jcpcr.jsp

stretching modes still dominate. Recall that the force constant analysis of the $^3B_1$ state at the MP2 level produced an imaginary frequency for the NO_2 antisymmetric stretch (AS). This mode is not included in the simulation for the $^3B_1$ state. If, in fact, there is a lower energy structure in C_s symmetry, which has not been investigated here, the NO_2 AS would be excited upon photodetachment in the simulated spectrum.

We now can compare the calculated energetics (Table VI) and simulated spectra to the data. In the 4.657 eV spectrum (Fig. 2), the position of peak A at 1.126 eV corresponds to a ADE of 3.531 eV. This lies between the calculated energies of the two lowest triplet states: the $^3A_2$ state (2.907 eV) and the $^3A_1$ state (4.278 eV). However, the simulated vibrational progression for the $^3A_2$ state at the HF level more closely resembles the experimental progression than that for any other triplet state. At the MP2 level, the agreement between the simulated and experimental intensity distribution is not as good, but both spectra are still are dominated by stretching rather than bending progressions. Moreover, the calculated and experimental (1240, 880, and 680 cm^{-1}) frequencies for the three symmetric modes are in better agreement than for the other triplet states. The band in the 4.657 eV spectrum is therefore assigned as the transition to the $^3A_2$ state.

In the 5.822 eV data, the progression beginning at peak A (eKE=1.286 eV) is in good agreement with the calculated result for the $^3A_1$ state not only energetically but also with respect to the appearance of the vibrational profile. Assuming peak A to be the 0–0 transition to the $^3A_1$ state, the experimental ADE is 4.536 eV which is reasonably close the calculated $^3A_1$ value of 4.278 eV. The simulations predict NO_2 bend excitation at both the HF and MP2 levels at a frequency ($\nu_3 \sim 600-650$ cm^{-1}) close to the observed value of 540 ± 40 cm^{-1}. The $^3B_2$ state is also a possibility based on comparing vibrational profiles, but since our highest level calculation (at the MP4 level) predicts this to be the highest energy of the four triplet states, the assignment of this progression to the $^3A_1$ state is more reasonable.

This progression continues under the two most intense features which appear in the spectrum. The positions of peaks D and G at 1.089 and 0.914 eV correspond to ADEs of 4.733 and 4.908 eV, which are both near the MP4 calculated ADE for the $^3B_1$ state (5.172 eV). Since no higher lying features are observed to indicate that the peaks belong to a single vibrational progression, peaks D and G may represent 0–0 transitions to two different electronic states which have geometries near that of the anion. Figures 5 and 6 show that only the $^3B_1$ simulation is dominated by the 0–0 transition while all of the other states considered here have long progressions and cannot explain the second intense feature. In this case, the second peak may result from transitions to an additional electronic state, either singlet or triplet, which has not been considered here. It is interesting to note that all of the structure observed in the spectrum lies well above the asymptotic energies for dissociation to $O+N_2O$ and $NO+NO$, and peaks F–K lie above not only the $N+NO_2$ but also the N_2+O+O dissociation asymptote. This will be further addressed in the next section.

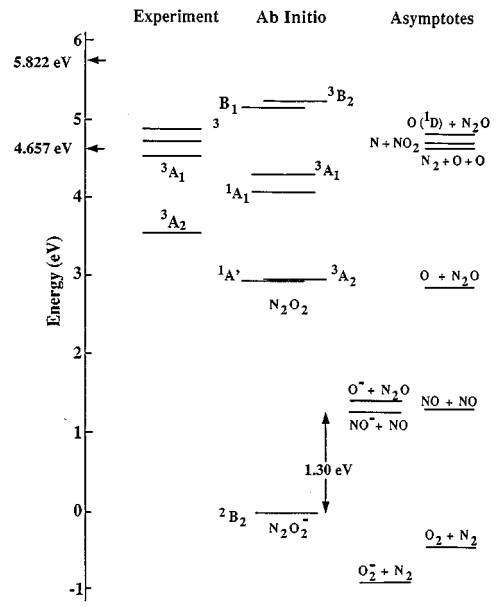

FIG. 7. Schematic energetics diagram for the $N_2O_2^-/N_2O_2$ system. Included are the *ab initio* calculated energies of the electronic states, the observed state origins, and the energetic asymptotes for dissociation of both the anion and the neutral.

B. Roles as reactive intermediates

Shown in Fig. 7 is a schematic energy diagram which summarizes the findings presented here and compares these results to the asymptotic energies of the separated reactants and products for both the anion and the neutral. All energies are with respect to the anion ground state, in eV. The left column indicates the experimentally observed transitions which have been assigned to 0–0 transitions in the 4.657 and 5.822 eV $N_2O_2^-$ photoelectron spectra. Arrows indicating the photon energies used in the experiments are shown against the left axis. The central column contains the energetic ordering of the electronic states according to the *ab initio* calculations at the MP4/6-311+G*//MP2/6-31+G* level of theory (including the ZPE correction). On the right are the anion and neutral dissociation asymptotes.

The photoelectron spectrum determines neutral energetics with respect to the $N_2O_2^-$ ground state, so the anion dissociation energy must be known in order to locate both the anion and neutral electronic states with respect to the various asymptotes. As illustrated in Fig. 7, the anion is bound with respect to dissociation to NO^-+NO by at most 1.3 eV. This value comes from a recent study in our laboratory of the photodissociation of $N_2O_2^-$.[48] The energy release resulting from $N_2O_2^-$ dissociation ($\lambda=500$ nm) in a fast (8 keV) ion beam was measured using a time-and-position sensitive coincidence detection scheme originally developed for free radical photodissociaton.[49] The limit for the dissociation is determined from the maximum observed kinetic energy release to both the O^-+N_2O and NO^-+NO dissociation channels. The dissociation energies determined from both channels, combined with the known reaction exothermicity, agree to within 10% (3 kcal/mol). A more complete description of these experiments will be provided in a future publication.

Downloaded¬03¬Mar¬2003¬to¬128.32.220.150. Redistribution¬subject¬to¬AIP¬license¬or¬copyright,¬see¬http://ojps.aip.org/jcpo/jcpcr.jsp

As discussed in Sec. I, the O^-+N_2O reaction is believed to proceed through this C_{2v} $N_2O_2^-$ intermediate, so our photodissociation result has characterized that well on the ion–molecule reaction surface. However, the rest of the anion reaction surface (see Fig. 1) remains uncharacterized. Thus, questions remain concerning the nature of the second minimum [i.e., for the $NO^-(NO)$ species] and the height of the barrier between the two minima and their role in the O^-+N_2O reaction.

In an early study of the $N+NO_2$ reaction,[15(a)] Clyne and Thrush proposed a C_{2v} NNO_2 structure as an intermediate for the reaction to form N_2O+O, and that this intermediate must exist long enough to undergo a significant rearrangement before dissociation to NO+NO, the dominant product of this reaction.[17] If a ground state $N(^4S)$ atom reacts with ground state NO_2 ($\tilde{X}\ ^2A_1$) along a C_{2v} reaction path, the $^3A_2$ state of the NNO_2 complex will be formed with a N–N single bond and unpaired electrons in the b_1 and b_2 orbitals (p orbitals localized on the terminal N atom). This is the $^3A_2$ state that we have assigned to the band in the 4.657 eV photoelectron spectrum. Figure 7 show that this state lies 1.4 eV below the $N+NO_2$ asymptote, so our photoelectron spectrum strongly supports the idea of a C_{2v} NNO_2 intermediate for this reaction.

Figure 7 also shows that the $^3A_2$ state lies above both the NO+NO and $O(^3P)+N_2O$ asymptotes. One certainly expects a significant barrier for dissociation of the $^3A_2$ state to NO+NO due to the substantial nuclear rearrangement required. Moreover, the $^3A_2$ state should not correlate diabatically to the $O(^3P)+N_2O$ channel, since the unpaired electrons must shift from the terminal N atom in the complex to the O atom in the separated products. Thus, again, a sizable barrier is expected. These considerations reinforce the notion that the NNO_2 complex is a local minimum on the reaction surface.

With regard to the higher lying states of N_2O_2 probed at 5.822 eV photodetachment energy, all peaks in Fig. 3 at lower electron kinetic energy than peak E correspond to states that can dissociate to $N+NO_2$ and N_2+2O in addition to the channels discussed above. The peaks are quite narrow up to and including peak J, after which the spectrum is far less structured, the only resolved feature being the broad peak K. This change in the appearance in the spectrum may reflect the onset of rapid dissociation, which could occur if, for example, there were a 0.56 eV barrier to dissociation for the $^3A_1$ state; this is the energy difference between peaks A and J in Fig. 3. However, given the complexity of this spectrum, this explanation should be considered tentative at best.

Finally, we compare our results to the $NO(v)+NO$ vibrational energy transfer study by Yang *et al.*[33] They observe the slope of the relaxation rate constant $k(v)$ to suddenly increase first at 2.2 eV of NO vibrational energy and then at 3.2 eV. They speculated that these discontinuities might arise due to the formation of metastable N_2O_2 collision complexes. Their energies are quite close to our experimentally determined energy differences between the $^3A_2$ and $^3A_1$ states, respectively, and the NO+NO asymptote, so it is possible that these low-lying triplet states play a role in the relaxation process. However, the $^1A'$ and $^1A_1$ singlet states are also in the right energy range, and the other structures calculated by Nguyen *et al.*[32] could also play a role. Nonetheless, our results represent the first experimental observation of N_2O_2 states that could contribute to the enhanced vibrational relaxation seen by Yang *et al.*

V. SUMMARY

We have presented the photoelectron spectra of $N_2O_2^-$ collected at $h\nu=4.657$ and 5.822 eV. By using the O^-+N_2O+M ion formation mechanism we are able to form exclusively the C_{2v} NNO_2^- species, as observed by Posey and Johnson.[9] The spectra contain resolved vibrational progressions for several electronic states of the neutral NNO_2 molecule. All of the observed features correspond to transitions to states of this species which are energetically unstable with respect to dissociation to at least three, and as many as six dissociation asymptotes. Our spectra thus represent the first observation of a high energy, chemically bound N_2O_2 species.

Ab initio calculations are presented for the geometries and vibrational frequencies of both the anion and neutral species. The $N_2O_2^-$ anion $\tilde{X}\ ^2B_2$ ground state is found to be planar with nearly equal bond lengths and bond angles. For N_2O_2, several electronic states which are accessible by one-electron photodetachment of the anion were investigated. Properties of the $^1A_1$, $^3A_2$, $^3A_1$, $^3B_2$, and $^3B_1$ (in C_{2v} symmetry) and $^1A'$ (in C_s symmetry) electronic states were calculated. At the highest level of theory considered, MP4/6-311+G*//MP2/6-31+G*, the lowest states, $^3A_2$ and $^1A'$, were found to be nearly isoenergetic. The remaining states were ordered energetically as $^1A_1<{}^3A_1<{}^3B_1<{}^3B_2$ at their respective equilibrium geometries. The calculations indicate that the triplet states are most likely to be observed in the photoelectron spectra based upon the geometry of each state with respect to the anion geometry. Simulated spectra are presented using the results of *ab initio* calculations for the lowest singlet and the four lowest triplet electronic states. Based on comparing these to the experimental spectra, the lowest and second lowest energy bands in the photoelectron spectra are assigned to transitions to the $^3A_2$ and $^3A_1$ states, respectively.

The anion and the neutral species studied here, $N_2O_2^-$ and N_2O_2, appear to be reactive intermediates in the O^-+N_2O and $N+NO_2$ reactions, respectively. The $^3A_2$ state in particular is a likely candidate for a reactive intermediate in the latter reaction. This state lies below the $N+NO_2$ asymptote but above the $O+N_2O$ and NO+NO channels. The observed vibrational structure indicates the existence of significant barriers to dissociation of the $^3A_2$ N_2O_2 complex which will play a role in the $N+NO_2$ reaction dynamics. This state and the other higher lying states observed in our spectra may also play a role in vibrational energy transfer from highly excited NO.

ACKNOWLEDGMENTS

Special thanks to D. J. Leahy and D. L. Osborn for determining D_0 ($N_2O_2^-$) upon request. This work has been sup-

Downloaded¬03¬Mar¬2003¬to¬128.32.220.150. Redistribution¬subject¬to¬AIP¬license¬or¬copyright,¬see¬http://ojps.aip.org/jcpo/jcpcr.jsp

ported by the United States Air Force Office of Scientific Research under Contract No. F49620-94-1-0115.

[1] A. G. Gaydon and H. G. Wolfhard, *Flames* (Wiley, New York, 1979).
[2] M. J. McEwan and L. F. Phillips, *Chemistry of the Atmosphere* (Wiley, New York, 1975).
[3] R. P. Wayne, *Chemistry of Atmospheres* (Oxford University Press, New York, 1985).
[4] R. F. Sawyer, *Eighteenth Symposium (International) on Combustion* (The Combustion Institute, Pittsburgh, 1980), p. 1.
[5] J. F. Paulson, Adv. Chem. Ser. **58**, 28 (1966); J. Chem. Phys. **52**, 959 (1970).
[6] J. L. Moruzzi and J. T. Dakin, J. Chem. Phys. **49**, 5000 (1968).
[7] S. E. Barlow and V. M. Bierbaum, J. Chem. Phys. **92**, 3442 (1990).
[8] R. A. Morris, A. A. Viggianio, and J. F. Paulson, J. Chem. Phys. **92**, 3448 (1990).
[9] L. A. Posey and M. A. Johnson, J. Chem. Phys. **88**, 5383 (1988).
[10] D. E. Milligan and M. E. Jacox, J. Chem. Phys. **55**, 3404 (1971).
[11] M. E. Jacox, J. Chem. Phys. **93**, 7622 (1990).
[12] J. Hacaloglu, S. Suzer, and L. Andrews, J. Phys. Chem. **94**, 1759 (1990).
[13] G. B. Kistiakowsky and G. G. Volpi, J. Chem. Phys. **27**, 1141 (1957).
[14] G. J. Verberke and C. A. Winkler, J. Phys. Chem. **64**, 319 (1960).
[15] M. A. A. Clyne and B. A. Thrush, Trans. Faraday Soc. **57**, 69 (1961); M. A. A. Clyne and I. S. McDermid, J. Chem. Soc. Faraday Trans. 1 **71**, 2189 (1975); M. A. A. Clyne and Y. Ono, Chem. Phys. **69**, 381 (1982).
[16] D. Husain and N. K. H. Slater, J. Chem. Soc. Faraday Trans. 2 **76**, 606 (1980).
[17] L. F. Phillips and H. I. Schiff, J. Chem. Phys. **42**, 3171 (1965).
[18] R. Iwata, R. A. Ferrieri, and A. P. Wolf, J. Phys. Chem. **90**, 6722 (1986).
[19] R. B. Metz, S. E. Bradforth, and D. M. Neumark, Adv. Chem. Phys. **91**, 1 (1992); D. M. Neumark, Accts. Chem. Res. **26**, 33 (1993).
[20] C. E. Klots and R. N. Compton, J. Chem. Phys. **69**, 1636 (1978).
[21] M. Knapp, O. Echt, D. Kreisle, T. A. Mark, and E. Recknagel, Chem. Phys. Lett. **126**, 225 (1986).
[22] J. V. Coe, J. T. Snodgrass, C. B. Friedhoff, K. M. McHugh, and K. H. Bowen, J. Chem. Phys. **87**, 4302 (1987).
[23] The numbering scheme follows that of Ref. 9.
[24] K. Hiraoka, S. Fujimake, K. Aruga, and S. Yamabe, J. Phys. Chem. **98**, 8295 (1994).
[25] W. A. Guillory and C. E. Hunter, J. Chem. Phys. **50**, 3516 (1969).
[26] S. G. Kukolich, J. Am. Chem. Soc. **104**, 4715 (1982); J. Mol. Spectrosc. **98**, 80 (1983).
[27] T.-K. Ha, Theoret. Chim. Acta **58**, 125 (1981).
[28] R. D. Harcourt, J. Mol. Struct. **206**, 253 (1990).
[29] H. H. Michels and J. A. Montgomery, Jr., J. Chem. Phys. **88**, 7248 (1988).
[30] R. D. Bardo, J. Phys. Chem. **86**, 4658 (1982).
[31] V. J. Zandwijk, R. A. J. Janssen, and M. H. Buck, J. Am. Chem. Soc. **112**, 4155 (1990).
[32] K. A. Nguyen, M. S. Gordon, J. A. Montgomery, Jr., and H. H. Michels, J. Phys. Chem. **98**, 10072 (1994).
[33] X. Yang, E. H. Kim, and A. M. Wodtke, J. Chem. Phys. **96**, 5111 (1992).
[34] R. B. Metz, A. Weaver, S. E. Bradforth, T. N. Kitsopoulos, and D. M. Neumark, J. Phys. Chem. **94**, 1377 (1990).
[35] M. A. Johnson, M. L. Alexander, and W. C. Lineberger, Chem. Phys. Lett. **112**, 285 (1984).
[36] R. Prosch and T. Trickl, Rev. Sci. Instrum. **60**, 713 (1989).
[37] W. C. Wiley and I. H. McLaren, Rev. Sci. Instrum. **26**, 1150 (1995).
[38] M. J. Frisch *et al.*, *Gaussian 92, Revision C* (Gaussian, Inc., Pittsburgh, PA, 1992).
[39] A. Weaver, D. W. Arnold, S. E. Bradforth, and D. M. Neumark, J. Chem. Phys. **94**, 1740 (1991).
[40] A. D. Walsh, J. Chem. Soc. **1953**, 2301.
[41] M. M. Maricq, J. J. Szente, Z. Li, and J. S. Francisco, J. Chem. Phys. **98**, 784 (1993); T. S. Dibble and J. S. Francisco, J. Phys. Chem. **98**, 11694 (1994).
[42] D. W. Arnold, S. E. Bradforth, E. H. Kim, and D. M. Neumark, J. Chem. Phys. **102**, 3493 (1995).
[43] M. Carlotti, J. W. C. Johns, and A. Trombetti, Can. J. Phys. **52**, 340 (1974).
[44] A higher level MCSCF calculation carried out in Ref. 32 predicts that the C_{2v} structure is a saddle point rather than a minimum, however.
[45] R. L. Reddington, W. B. Olson, and P. C. Cross, J. Chem. Phys. **36**, 1311 (1962).
[46] Y. Morino, T. Iijima, and Y. Murata, Bull. Chem. Soc. Jpn. **33**, 46 (1960).
[47] For the $^3B_1$ state, this value is reported even though the force constant analysis at the MP2 level indicates that it is a saddle point species.
[48] D. L. Osborn, D. J. Leahy, and D. M. Neumark (to be published).
[49] R. E. Continetti, D. R. Cyr, D. L. Osborn, D. J. Leahy, R. B. Metz, and D. M. Neumark, J. Chem. Phys. **99**, 2616 (1993).

Downloaded¬03¬Mar¬2003¬to¬128.32.220.150. Redistribution¬subject¬to¬AIP¬license¬or¬copyright,¬see¬http://ojps.aip.org/jcpo/jcpcr.jsp